where the prime indicates that the sum over α is restricted to the chosen configuration. This is the self-consistent potential used in the W.B.B. treatment.

In the τ matrix expansion shown in Eq. (17) the comparison potential U no longer appears explicitly, so that the usual self-consistent definition of U will be of no use. But there is a weaker kind of self-consistency condition which can be invoked for the τ matrix expansion. This consists in defining U to be any convenient sum of one-body potentials which have one parameter free. This parameter could be the depth or the range of these potentials. This parameter is then adjusted so that the first-order term of the level shift-expansion, $\langle\sum\tau_\alpha\rangle$, vanishes. While this type of self-consistent potential cannot be expected to be as effective as the Hartree-Fock or W.B.B. types in increasing the initial rate of convergence of the perturbation expansion, it certainly is much easier to implement.

VI. ACKNOWLEDGMENTS

The author is greatly indebted to Professor R. E. Peierls for a great deal of constructive criticism in the course of this investigation. He is indebted also to J. Lascoux and C. de Dominicis for many helpful discussions on this topic. Finally he wishes to thank the Department of Mathematical Physics at the University of Birmingham for the hospitality he has received.

PHYSICAL REVIEW VOLUME 107, NUMBER 1 JULY 1, 1957

Appreciation of a Velocity-Dependent Potential to the Nuclear Photoeffect*

S. RAND†
University of California, Berkeley, California
(Received September 10, 1956)

Calculations of the total photonuclear absorption cross sections have been carried out for a number of nuclei throughout the periodic table. The shell model, with a velocity-dependent potential, has been used. This potential is proportional to the kinetic energy of the nucleons, and gives rise to a changed effective nucleon mass. One of the effects of such an effective mass is to change the frequencies of the giant gamma-ray absorption resonances. Previous independent-particle model calculations had resulted in frequencies consistently lower than the observed values.

With an effective nucleon mass inside the nucleus of about 55% of the normal mass, very good agreement with the experimental values is obtained for medium and heavy nuclei. Within the limits of the assumptions made in the calculations, the forms of the observed excitation curves are closely reproduced, and are peaked at roughly the correct energies. Furthermore, the cross sections integrated over excitation energies, which are nearly model-independent quantities in the changed-mass case, are, except for the very light nuclei, consistent with the experimental values.

I. INTRODUCTION

A NUMBER of models have been proposed[1] in order to explain the giant resonance phenomena of the photonuclear effect.[2,3] It has been pointed out by Levinger[1] that there is little difference between the predictions of all reasonable sub-unit models. Recently however, some magic-number phenomena relating to the photoeffect have been observed. In particular, the resonance widths for closed-shell nuclei are smaller than the widths for neighboring nuclei. Since the shell model has been fairly successful in predicting the properties of the ground states,[4] and the low-lying excited states,[5] it is reasonable to attempt an extension of the model to higher levels. Such proposals have been made by Wilkinson,[6] Courant,[7] Burkhardt,[8] and others.[9,10]

If we assume only ordinary (space-dependent) forces to exist between nucleons, photoabsorption is not satisfactorily explained by the independent-particle model. The principal discrepancies are:

1. The calculated transition energies are smaller by about 50% than the observed resonance energies.[6]

2. Photon scattering provides major competition to neutron emission. This is not observed.[8]

3. The resonance frequencies depend too strongly on mass number.[6]

* Supported in part by the Office of Ordnance Research, U. S. Army.

† Now at the Institute of Mathematical Sciences, New York University, New York City.

[1] J. S. Levinger, *Annual Reviews of Nuclear Science* (Annual Reviews, Inc., Stanford, 1955), Vol. 4.

[2] Montalbetti, Katz, and Goldemberg, Phys. Rev. **91**, 659 (1953).

[3] R. Nathans and J. Halpern, Phys. Rev. **93**, 437 (1954).

[4] M. G. Mayer and J. H. D. Jensen, *Elementary Theory of Nuclear Shell Structure* (John Wiley and Sons, Inc., New York, 1955).

[5] D. R. Inglis, Revs. Modern Phys. **25**, 390 (1953).

[6] D. H. Wilkinson, *Proceedings of the 1954 Glasgow Conference on Nuclear and Meson Physics* (Pergamon Press, London and New York, 1955), pg. 161.

[7] E. D. Courant, Phys. Rev. **82**, 703 (1951).

[8] J. L. Burkhardt, Phys. Rev. **91**, 420 (1953).

[9] A. Reifman, Z. Naturforsch. **8a**, 505 (1953).

[10] S. S. Wu, doctoral thesis, University of Illinois, 1951 (unpublished).

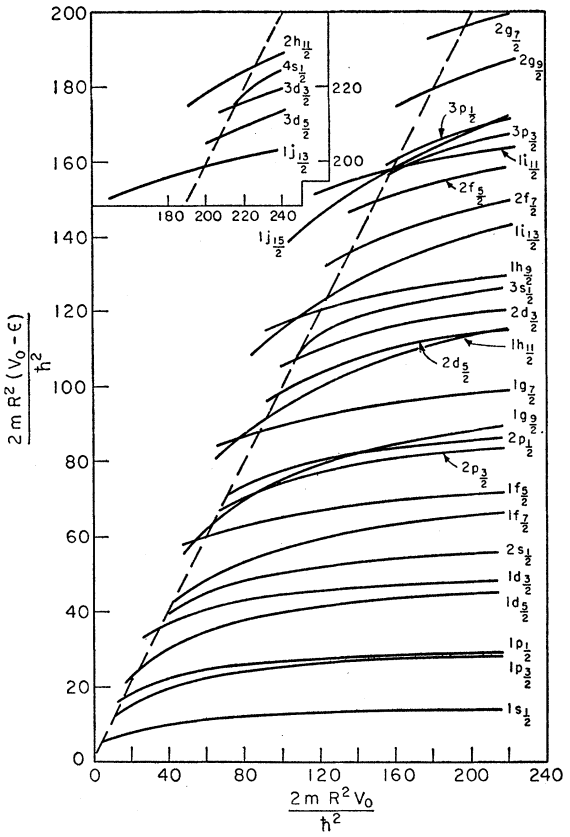

FIG. 1. Single-particle energy levels for particles governed by the Hamiltonian $H=(1/2m)[\mathbf{p}K\cdot\mathbf{p}+i\boldsymbol{\sigma}\cdot\mathbf{p}K\times\mathbf{p}]+V$, where

$V=-V_0$ for $r<R$
$=0$ for $r>R$;
$K=1.8$ for $r<R$
$=1$ for $r>R$.

The axes are labeled by the dimensionless parameters $2mR^2V_0/\hbar^2$ and $2mR^2(V_0-\epsilon)/\hbar^2$, where ϵ is the binding energy.

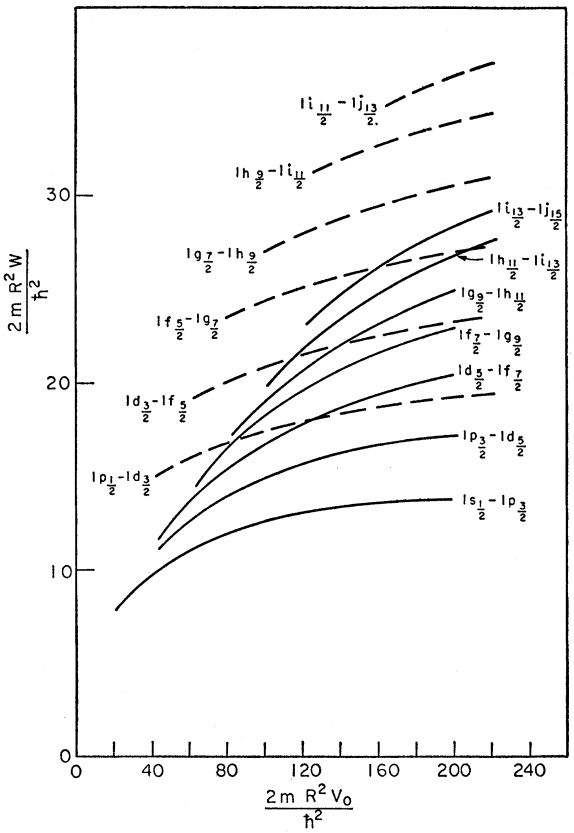

FIG. 2. Electric dipole transition energies between levels for which the particle wave functions have no radial nodes. Solid curves represent transitions of the type $1l_{j=l+\frac{1}{2}}\rightarrow 1(l+1)_{j=l+1+\frac{1}{2}}$ that is, for spin and orbital angular momenta parallel. Dashed curves are for $1l_{j=l-\frac{1}{2}}\rightarrow 1(l+1)_{j=l+1-\frac{1}{2}}$. The parameter $2mR^2W/\hbar^2$ is used for the vertical axis, where W is the transition energy.

4. The model-independent dipole sum predicts values for the cross sections integrated over frequencies which are too small.[11]

We have considered the problem using a velocity-dependent potential of the types introduced by Johnson and Teller[12] and by Duerr.[13] The nonrelativistic expansion of Duerr's Hamiltonian is

$$H=(1/2m)\mathbf{p}K\cdot\mathbf{p}+(i/2m)\boldsymbol{\sigma}\cdot\mathbf{p}K\times\mathbf{p}+V, \quad (1)$$

where $K\equiv m/m_{\text{eff}}=1/(1-\varphi)$ and $V=U-mc^2\varphi$. Here φ is a (dimensionless) scalar potential, and U is the fourth component of a vector potential. The effective mass inside the nucleus is written as m_{eff}.

II. METHOD

In our calculations, we have made the following approximations:

1. The potentials φ and U are square-well potentials, with $\varphi\approx 0.45$ inside the nucleus and 0 outside, so the $K=m/m_{\text{eff}}=1.8$ inside. This gives Duerr's value for m_{eff}.[13] The quantity $V=U-mc^2\varphi$ is taken to have a value inside the nucleus such that the correct number of particles are bound with the observed binding energies.
2. The Coulomb effect is taken into account only to the extent that the velocity-independent potential well is more shallow for protons than for neutrons.
3. All levels within a shell-model configuration are degenerate.
4. Only electric dipole transitions are considered.
5. The nonrelativistic Hamiltonian of Eq. (1) is used.

No further considerations will be given to the first two approximations. In Sec. IV, however, along with a consideration of pairing energies, we shall improve on the last three approximations.

In Fig. 1 we have plotted the single-particle energy levels as a function of the velocity independent potential well depth. In Fig. 2 are the transition energies for single-particle dipole transitions in which the initial

[11] J. S. Levinger and H. A. Bethe, Phys. Rev. **78**, 115 (1950).
[12] M. Johnson and E. Teller, Phys. Rev. **98**, 783 (1955).
[13] H. P. Duerr, Phys. Rev. **103**, 469 (1956).

and final wave functions have no radial nodes (other than those at the origin and at infinity).

The dipole transition probabilities were calculated with a well-known formula. The matrix elements of the electric dipole moment were determined by an extension of a method introduced by Courant.[7] The result is

$$\ddot{z}_{\alpha\beta}=-\omega_{\alpha\beta}^2 z_{\alpha\beta}$$
$$=-\frac{1}{m}(\cos\theta)_{\alpha\beta}\left\{\frac{d}{dr}(KV)-[E+\tfrac{1}{2}(1-\delta)W]\frac{dK}{dr}\right.$$
$$-\frac{\hbar^2}{2m}\Big[(\delta+2n+2)K\frac{dK}{dr}\frac{1}{r}\frac{d}{dr}$$
$$+[n-(\boldsymbol{\sigma}\cdot\mathbf{l})_{\alpha\alpha}]\frac{d}{dr}\Big(\frac{1}{r}K\frac{dK}{dr}\Big)$$
$$\left.-[n\delta+2l(l+1)]\frac{1}{r^2}K\frac{dK}{dr}\Big]\right\}_{\alpha\beta}, \quad (2)$$

where E is the energy of state α, W is the transition energy, $\delta\equiv(\boldsymbol{\sigma}\cdot\mathbf{l})_{\beta\beta}-(\boldsymbol{\sigma}\cdot\mathbf{l})_{\alpha\alpha}$, and

$$n=l \quad \text{for transitions} \quad j\to j+1,\ l\to l+1$$
$$=-l-1 \quad \text{for transitions} \quad j\to j-1,\ l\to l-1.$$

All terms on the right hand side of (2) are matrix elements of δ functions and are easily evaluated with the square-well wave functions.

In accordance with the cloudy crystal ball model,[14] each of the spectral lines was broadened by roughly 3 Mev to account for particle interactions. Lines resulting from transitions to virtual states were further broadened to take account of the finite lifetime of the excited states against direct particle emission. Transitions to the continuum (energy of the excited states exceeds its centripetal energy) contributes to a broad high-energy background rather than to the giant resonance, and were not included in plots of the excitation curves. These latter contributions however, amounted to about 15% of the total strength, and were included in calculations of the integrated cross sections. Natural line broadening is negligible in all cases.

TABLE I. Velocity-independent potential well depths for various nuclei, with a nuclear radius of $1.2\times10^{-13}A^{\frac{1}{3}}$ cm.

Nucleus	V_0 (neutrons) Mev	V_0 (protons) Mev	Nucleus	V_0 (neutrons) Mev	V_0 (protons) Mev
U^{238}	64	54	Rh^{103}	76	60
Bi^{209}	68	58	Nb^{93}	78	64
Au^{197}	68	60	As^{75}	73.5	61
Ta^{181}	72.5	59	Mn^{55}	70	60
La^{139}	73	62	P^{31}	68	68
I^{127}	72	64	Mg^{24}	70	70

[14] Feshbach, Porter, and Weisskopf, Phys. Rev. **96**, 448 (1954).

As a second evaluation of the summed dipole strengths we used the sum rule

$$\int\sigma dW=\frac{2\pi^2\hbar}{mc}\sum_P e_P\sum_\alpha K_{\alpha\alpha}(P), \quad (3)$$

where the e_P are the effective charges for dipole transitions,[15] and as before, $K\equiv m/m_{\text{eff}}$; P refers to the two types of nucleons.

III. RESULTS

In Table I are listed the values of the velocity-independent potential well depths for both kinds of nucleons using nuclear radii $R=1.2A^{\frac{1}{3}}\times10^{-13}$ cm. The values are chosen so that the correct number of particles are bound by the observed binding energies. However the results obtained are almost entirely independent of the choice of these well depths. They have no effect on the integrated cross sections, and make very little difference in the transition energies.

In Table II we have presented a sample of the data used for obtaining the excitation curves. The first two columns of Table II give the initial levels that can contribute, and the number of nucleons in these levels. The data have been taken from the ground-state configuration assignments given by Mayer and Jensen.[16] The next two columns list the final levels that can be

TABLE II. Au^{197}. An example of the calculated data for a particular nucleus.

Level α	N_α	Level β	F_β	$N_\alpha F_\beta\int\sigma_{\alpha\beta}dW$ Mev b	$2mR^2W/\hbar^2$	Form
		Neutrons	$V_0=68$ Mev			
$1i_{13/2}$	12	$1j_{15/2}$	1	0.465	26.0	C_1
		$2h_{11/2}$	1	0.075	78.0	B
$2f_{5/2}$	6	$2g_{7/2}$	1	0.21	36.6	C_1
		$3d_{3/2}$	1	0.06	51.0	B
$2f_{7/2}$	8	$2g_{9/2}$	1	0.255	31.5	C_1
		$3d_{5/2}$	1	0.11	54.0	B
$1h_{9/2}$	10	$1i_{11/2}$	1	0.405	32.3	C_1
		$2g_{7/2}$	1	0.05	63.6	C_2
$3s_{1/2}$	2	$3p_{7/2}$	1	0.05	35.8	C_1
$2d_{3/2}$	4	$3p_{1/2}$	1	0.05	44.0	C_2
$1h_{11/2}$	12	$1i_{13/2}$	2/14	0.06	24.8	C_1
		$2g_{9/2}$	1	0.075	66.6	C_2
$2d_{5/2}$	6	$3p_{1/2}$	1	0.08	46.5	C_2
				Sum = 1.945		
		Protons	$V_0=60$ Mev			
$2d_{3/2}$	3	$2f_{5/2}$	1	0.20	33.2	C_1
		$3p_{1/2}$	1	0.08	40.5	B
$1h_{11/2}$	12	$1i_{13/2}$	1	0.93	23.4	C_1
		$2g_{9/2}$	1	0.17	65.0	B
$2d_{5/2}$	6	$2f_{7/2}$	1	0.35	29.4	C_1
		$3p_{3/2}$	1	0.18	43.0	B
$1g_{7/2}$	8	$1h_{9/2}$	1	0.635	28.7	C_1
		$2f_{5/2}$	1	0.095	53.0	B
$1g_{9/2}$	10	$2f_{7/2}$	1	0.14	56.5	C_2
$2p_{1/2}$	2	$2d_{3/2}$	1/4	0.03	31.6	C_1
$1f_{5/2}$	6	$2d_{3/2}$	1/4	0.02	45.0	C_2
$2p_{3/2}$	4	$3s_{1/2}$	1	0.125	39.0	C_2
				Sum = 2.955		

[15] H. A. Bethe, Rev. Modern Phys. **9**, 87–90, 71 (1937).
[16] Reference 4, Chap. 5.

TABLE III. Summary of calculated and experimental data. Calculations were carried out using the approximations described in Sec. II.

	1. $\int\sigma dW$(calc) Mev-b	2. $\int\sigma$(res) $\times dW$(calc) Mev-b	3. $\int_0^{25}\sigma(\gamma,n)$ $\times dW$(exp) Mev-b	4. $\bar{W}$(calc) Mev	5. W_{max}(calc) Mev	6. W_{max}(exp) Mev	7. Γ_c Mev	8. Γ(calc) Mev	9. Γ(exp) Mev	10. σ_{max}(calc) barns	11. σ_{max}(exp) barns
U^{238}	5.74	4.21	4.55	14.15	12.2	13.8[a]	3.40	5.7	6.6	0.49	0.98
Bi^{209}	5.12	3.79	4.08	14.9	12.0	13.2	3.31	5.6	4.1	0.44	0.63
Au^{197}	4.90	3.59	3.19	14.95	11.75	13.9	3.43	5.7	6.9	0.41	0.456
Ta^{181}	4.45	3.27	3.43	15.25	12.05	15.1	3.18	5.6	7.9	0.37	0.397
La^{139}	3.48	2.65	?	16.7	13.9	15.5	3.26	6.9	5.7	0.267	?
I^{127}	3.22	2.39	2.04	17.2	13.8	16.5	3.45	6.8	8.3	0.23	0.243
Rh^{103}	2.65	1.91	1.94	18.4	14.2	17.0	3.31	6.55	8.9	0.187	0.205
Nb^{93}	2.43	1.72	1.46	18.9	15.6	17.3	3.19	6.9	6.8	0.169	0.195
As^{75}	1.90	1.43[b]	0.80	19.95	16.45[b]	18.4	4.08	9.8	9.0	0.105	0.0903
Mn^{55}	1.39	0.99	0.88	19.85	16.7	21.5	4.01	7.7	8.8	0.101	0.0969
P^{31} [c]	0.816	0.456	0.161	24.2	17.9	21.5	3.58	3.7	10.2	0.0705	0.0167
	0.816	0.545[d] 0.410[e]	0.161	24.2	19.0		8.6	10.0	10.2	0.035	0.0167
Mg^{24}	0.580	0.406[f]	0.055[g] 0.16[g]	26.2	21.1	19.5	8.73	11.0	7–8	0.025	0.0084

[a] Includes $(\gamma,2n)$ and (γ,f) weighted according to the number of neutrons emitted.
[b] Includes two peaks, believed to be unresolved experimentally.
[c] The first set of values were determined by using a collision width $\Gamma_c=3.58$ Mev. For the second set, a collision width $\Gamma_c=8.6$ Mev was used.
[d] Value given for $\int_0^{25}\sigma dW$.
[e] Value given for $\int_0^{22.5}\sigma dW$.
[f] $\int_0^{25}\sigma dW=0.271$ Mev-b.
[g] The two values given are for $\int_0^{24}\sigma(\gamma,n)dW$(exp) and $\int_0^{28}\sigma(\gamma,p)dW$(exp), respectively.

reached by means of dipole transitions, and the fraction of these levels that are initially empty. Possible transitions to levels other than those specifically listed have been found to give rise to negligible contributions. In the fifth column are the integrated cross sections for the single particle transitions, multiplied by the number of particles in the initial level and by the fraction of holes in the final level. (We have treated levels within a configuration as degenerate.) In the next column, we have listed the values of the parameters $2mR^2W/\hbar^2$ corresponding to the transition energies, some of which have been taken from Fig. 2.

Listed in column 7 are the categories chosen for the excited level widths. The symbols C_1 or C_2, are used depending on whether the transition will contribute to the giant resonance or to a subsidiary resonance. For those cases where the width for particle escape (Γ_P) is much greater than the collision width (Γ_c) the symbol B is written to designate that the transition is one contributing to a background. In the few cases that $\Gamma_p\approx\Gamma_c$, the total width for the transition, $\Gamma_p+\Gamma_c$ is listed. In the seventh column of Table III we have given the collision width Γ_c assumed for each nucleus.

Figure 3 shows the cross sections as functions of the transition energy for three sample nuclei. Similar curves for a number of other nuclei have not been included. The solid curves labeled (a) represent the cross sections calculated using the methods of this section. A discussion of the methods used to arrive at the curves (b) will be given in Sec. IV. The dashed curves are experimental, and include (γ,n) processes only. The bottom and left hand scales correspond to nuclear radii $1.2\times10^{-13}A^{\frac{1}{3}}$ cm, taken to be the same for both neutron and proton cores. The top and right hand scales result from radii of $1.3\times10^{-13}A^{\frac{1}{3}}$ cm.

The interesting data taken from these and other graphs are given in Table III, and the corresponding experimental results are also shown for comparison. All of the experimental data are taken from the work of Nathans and Halpern,[3] except where indicated otherwise.

We use the following notation:

Total integrated electric dipole cross section$\equiv\int\sigma dW$.

Cross section integrated over the giant resonance $\equiv\int\sigma(\text{res})dW$.

Cross section integrated to energy b in Mev$\equiv\int_0^b\sigma dW$.

Mean energy$\equiv\int_0^\infty\sigma W dW/\int_0^\infty\sigma dW=\bar{W}$.

Energy at which cross section of the giant resonance is a maximum$\equiv W_{max}$.

Individual level collision width assumed$\equiv\Gamma_c$.

Width of the giant resonance at half-maximum$\equiv\Gamma$.

Maximum cross section of the giant resonance$\equiv\sigma_{max}$.

The results that we have obtained in this section indicate a general improvement over previous independent-particle-model calculations. The integrated cross sections have been increased over results obtained by using purely space-dependent forces, and except for the very light nuclei, are no longer inconsistent with the experimental results. Furthermore, the transition energies are also increased, and the agreement here is again greatly improved.

We note that the introduction of an appropriately chosen percentage of Majorana exchange force can also result in good agreement with observed integrated cross sections.[11] Unfortunately, further comparison with exchange force calculations is not possible since other

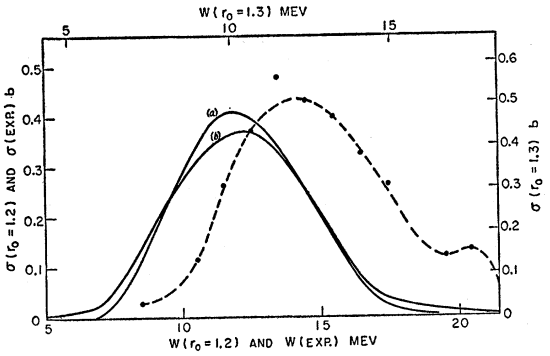

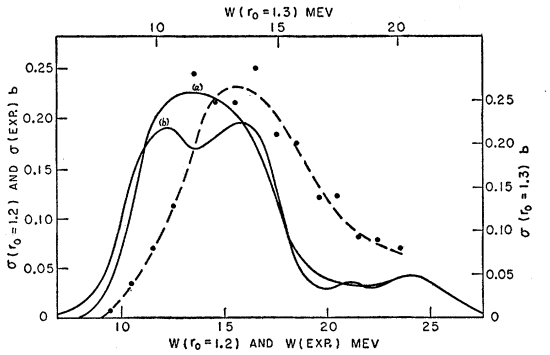

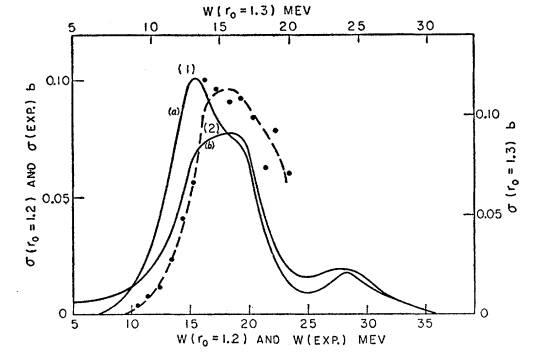

FIG. 3. Total electric dipole cross sections as functions of excitation energy for the absorption of γ rays by various nuclei. (A) Au^{197}. (B) I^{127}. (C) Mn^{55}. The solid curves are the calculated cross sections. The dots are experimental points for the (γ,n) process, taken from Nathans and Halpern.[3] The curves drawn through the experimental points are not those of Nathans and Halpern. The scales at the left and at the bottom correspond to calculations made with nuclear radii, $R=1.2\times10^{-13}A^{\frac{1}{3}}$ cm. These scales also refer to experimental curves. The scales at the right and at the top correspond to calculations made with nuclear radii, $R=1.3\times10^{-13}A^{\frac{1}{3}}$ cm.

consistent calculations are lacking. The mean energies, $\overline{W}$, have been determined by Levinger and Bethe,[11] but their treatment neglected Pauli-principle correlations. In a later paper by Levinger and Kent,[17] it is demonstrated that this procedure may not be permissible.

[17] J. S. Levinger and D. C. Kent, Phys. Rev. **95**, 418 (1954).

With reference to the first three numbered columns of Table III, it might appear that we have calculated integrated cross sections that are in general too large. Very close agreement can hardly be expected, however, because neither the values given in column 1 nor those in column 2 are precisely the quantities that were measured. In particular, only emitted neutrons were observed in the experiments and therefore column 3 gives (γ,n) cross sections. For heavy nuclei, the resulting integrated cross sections are roughly 10% less than the corresponding value for total absorption, the difference being due to low-energy (γ,γ) elastic and inelastic scattering.[18,19] For light nuclei, however, the difference is much greater. The relatively small Coulomb potential is no longer effective in preventing proton emission, and the (γ,p) process becomes prominent. Measurements[20,21] on Mg^{24} indicate that the (γ,p) effect is almost three times as important as neutron emission, although this is probably an extreme case.

Comparing columns 5 and 6, it is seen that the calculated resonance energies are almost invariably too small. The discrepancies average to almost 2 Mev (see also Fig. 4). It will now be shown that the inclusion of a number of small-order corrections makes the agreement almost complete.

IV. SMALL-ORDER CORRECTIONS

Effects Due to Relativistic Corrections

Relativistic terms in the Hamiltonian cause a considerable reduction in the transition energies and in the integrated cross sections. All energy levels of Fig. 1 are lowered because of the relativistic increase in mass. However, more energetic ones have a greater decrease in energy than less energetic ones, so that the energy levels are closer together. With the velocity-dependent potential, both the relativistic decreases in transition energies and integrated cross sections turn out to be about 10% for all nuclei.

The following approximations were used:

1. In all relativistic correction terms, we have neglected surface terms, that is, terms involving the commutators of p and m_{eff}.

2. In all correction terms, we treated the nucleons as if they were entirely within the nucleus.

The resulting formulas are as follows.

A modified sum rule:

$$\int\sigma^R dW=\frac{2\pi^2\hbar}{mc}\sum_P e_P^2\sum_\alpha K_{\alpha\alpha}\left(1+\frac{2a^2T_\alpha}{mc^2}\right)^{-\frac{3}{2}}\times\left(1+\tfrac{2}{3}\frac{2a^2T_\alpha}{mc^2}\right). \quad (4)$$

[18] M. B. Stearns, Phys. Rev. **87**, 706 (1952).

[19] E. G. Fuller and E. Hayward, U. S. National Bureau of Standards Report 3129, 1954 (unpublished).

[20] R. Nathans and P. F. Yergin, Phys. Rev. **98**, 1926 (1955).

[21] S. A. N. Johansson, Phys. Rev. **97**, 1186 (1955).

Transition energy between two single-particle levels:

$$W_{\alpha\beta}{}^{R}=\left(1+\frac{a^2(T_\alpha+T_\beta)}{mc^2}\right)^{-\frac{1}{2}}W_{\alpha\beta}. \quad (5)$$

Integrated cross section for a transition between two single-particle levels:

$$\sigma_{\alpha\beta}{}^{R}dW=\left(1+\frac{a^2(T_\alpha+T_\beta)}{mc^2}\right)^{-\frac{1}{2}}\sigma_{\alpha\beta}dW. \quad (6)$$

T_α is the kinetic energy of a particle in state α when it is entirely inside the nucleus, and $a=(m/m_{\text{eff}})_{\text{inside}}=1.8$.

Effects Due to Pairing Energies

A consideration of pairing energies is fundamental to our method of treating the problem, since almost all transitions which we have considered involve the breaking of a nucleon pair. In all cases, the pairing energies tend to raise the energies of the giant resonances.

In Table IV we have listed a few nuclei, along with the results obtained in Sec. III for the resonance energies. In the third column we have subtracted 10% to account for the relativistic effects discussed in the first part of this section. The next column contains the initial levels that contribute most to the giant resonances, along with the proposed pairing energies and percentage contributions in parentheses. (Except for light nuclei, it is not possible to obtain a consistent estimate of the pairing energies. We have used Mayer and Jensen's values for the magnitudes of the pairing energies for the $1d_{5/2}$, $1d_{3/2}$, and $1f_{7/2}$ neutron levels in nuclei with neutron numbers 8 to 28.[22]) We have not distinguished between neutron and proton levels, and have assumed their pairing energies to be the same. In the last column, the experimental resonance energies are listed.

The nucleus P^{31} represents an extreme example of the importance of pairing energies. We note that a great majority (87%) of the transitions originate from the level $1d_{5/2}$ with a pairing energy of 3.7 Mev. If it were assumed that all transitions originated from this level, then the predicted resonance energy would be 17.1+3.7 = 20.8 Mev, in good agreement with the experimental value of 21.5 Mev.

TABLE IV. Effects of pairing energies among light nuclei. (Energies in Mev.)

Nucleus	Non-relativistic resonance energy	Relativistic resonance energy	Principal level and percentage	Exper. res. energy
Mg^{24}	21.1	19.0	$1d_{5/2}$ (3.7 Mev, 42.5%)	19.5
P^{31}	19.0	17.1	$1d_{5/2}$ (3.7 Mev, 87%)	21.5
Mn^{55}	16.7	15.0	$1f_{7/2}$ (3.2 Mev, 51.5%) $1d_{3/2}$ (2.9 Mev, 31%)	18.4
As^{75}	16.45	14.8	$1f_{7/2}$ (3.2 Mev, 37.5%)	17.3

[22] Reference 4, Chap. 2.

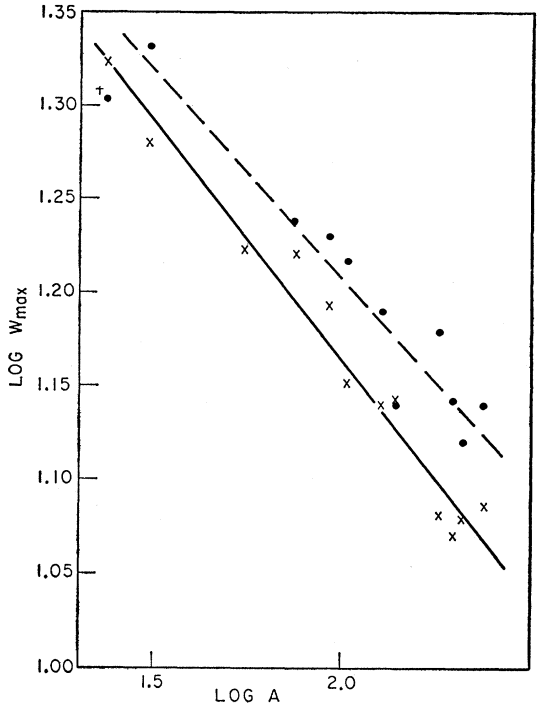

FIG. 4. A log-log plot of resonance energy *vs* nuclear mass number. The crosses represent calculated points using nuclear radii of $1.2\times10^{-13}A^{\frac{1}{3}}$ cm, and the circles are experimental points. The best straight lines have been drawn through each set of points.

Effects Due to Quadrupole Transitions

To determine the extent to which quadrupole transitions contribute, we used the quadrupole sum rule,

$$\int\sigma(E2)\frac{dW}{W^2}=\frac{\pi^2e^2}{3hmc^3}\sum_{\text{protons}}(\text{Kr}^2)\approx\frac{1.8\pi^2e^2ZR^2}{5hmc^3}. \quad (7)$$

If the major contributions for the quadrupole transitions occur at roughly the same energies as for dipole transitions, then the resulting integrated cross sections that we have determined are increased by only about $3\frac{1}{2}$%. Since quadrupole energies are believed to be somewhat smaller than the energies of the giant dipole resonances, this estimate of the quadrupole contribution may possibly be too large. In either case, we feel justified in neglecting quadrupole effects, even as a first-order correction.

Effects Due to Valence Transitions

Throughout the treatment of the problem we have neglected pairwise forces; that is, we have assumed that all energy levels within a shell model configuration are degenerate. It will now be assumed that identical particles may interact, resulting in a removal of the

TABLE V. Effects of interparticle forces on the calculated data. Unprimed quantities are those given by the original calculations. Primed quantities include the effects of the coupling, as described in section on small order corrections, sub-section effects due to valence transitions.

Nucleus	Γ (calc) Mev	Γ' (calc) Mev	Γ (exp) Mev	W_{max} (calc) Mev	W_{max}' (calc) Mev	W_{max} (exp) Mev	σ_{max} (calc) barns	σ_{max}' (calc) barns	σ_{max} (exp) barns
Au^{197}	5.7	6.2	6.9	11.75	12.2	13.9	0.41	0.37	0.456
Ta^{181}	5.6	6.45	7.9	12.05	13.55	15.1	0.37	0.26	0.397
I^{127}	6.8	7.75	8.3	13.8	14.65	15.5	0.23	0.20	0.243
Rh^{103}	6.55	6.0	8.9	14.2	14.8	16.5	0.187	0.180	0.205
As^{75}	9.8	9.5[a]	9.0	16.45	16.3	17.3	0.105	0.114	0.0903
Mn^{55}	7.7	7.8	8.8	16.7	18.0	18.4	0.101	0.077	0.0969

[a] For As^{75} the collision width Γ_c has been reduced from 4.08 Mev to 3.27 Mev in making the revised calculation.

degeneracy. The assumption that only identical particles interact is very good for heavy nuclei. For light nuclei, however, when neutron and proton shells are filling simultaneously, this assumption is not entirely justified.

This inclusion of particle interactions has the expected effect of widening the giant resonances. It is found that it also raises the resonance energies.

To determine the effects of these valence transitions on the excitation curve, a number of approximations are necessary. We have assumed that the energy levels of the final configuration are separated by one Mev, and that they are centered about the single particle configuration energy. Furthermore, the transition probabilities from the ground state to each of these levels are taken to be equal, so that the transition probability to each level is equal to the single-particle transition probability divided by the number of levels. We have further assumed normal coupling for all ground states.

The resulting excitation curves have been determined for a number of nuclei in which valence transitions appear to play a prominent role. Three of these are the solid curves labeled (b) in Fig. 3.

In Table V we have listed the results. The unprimed quantities are those that were previously calculated, and which are given in Table IV. The primed quantities are those obtained by the inclusion of j-j coupling.

Perhaps a surprising result is the systematic effect of the pairwise coupling on the resonance energies. The effect is almost invariably an increase in the resonance energies, resulting in better agreement with the experimental values.

V. CONCLUSIONS

The inclusion of small-order corrections has improved nearly all of our results obtained in the previous section. Considering the approximate nature of our treatment, it is apparent that the shell model with the velocity-dependent potential is able to account for the photonuclear effect in heavy nuclei quite satisfactorally.

The integrated cross sections of Table III can be altered only by changing the momentum dependence of the Hamiltonian. Thus, the only small-order correction that can change those results is due to the inclusion of relativity. It is shown that there is a resulting reduction of 10%. This reduction allows for the possibility of complete agreement between calculated and observed integrated cross sections, except possibly for light nuclei.

The resonance energies of Table III are affected by a number of small-order corrections. Our first set of calculations yielded results too small by slightly less than 2 Mev. The relativistic treatment resulted in further disagreement, the average discrepancy being increased to about 3 to 3.5 Mev. However, it was then demonstrated that both the effect of pairing energies, and a more accurate treatment of valence transitions increase the resonance energies, and can remove this discrepancy entirely. An average pairing energy of about 2 to 2.5 Mev was shown to be plausible from experimental data. The balance of 1 Mev is explained by the effect of valence transitions.

It should be remarked that agreement to within 1 Mev would be fortuitous, since the use of more realistic nuclear potentials, and a more accurate treatment of the Coulomb effect can easily account for 1 Mev. These last two effects have not been included in our work.

VI. ACKNOWLEDGMENTS

I am deeply indebted to Professor Edward Teller for suggesting this problem to me, and for his continued guidance and encouragement throughout the course of the investigation.

I would also like to thank Dr. Hans Mark for the time and effort he spent in reading the final draft and for the many helpful suggestions that resulted. Thanks are also due to Dr. R. D. Lawson and Dr. R. Huddlestone for many stimulating comments and criticisms.